coatings

MDPI

Article

Enhancing Coating Adhesion on Fibre-Reinforced Composite by Femtosecond Laser Texturing

Filomena Piscitelli [1], Raffaele De Palo [2,3] and Annalisa Volpe [2,3,*]

[1] Italian Aerospace Research Centre, CIRA, Via Maiorise, 1, 81043 Capua, Italy; f.piscitelli@cira.it
[2] Dipartimento Interateneo di Fisica, Politecnico di Bari & Università degli Studi di Bari, 70125 Bari, Italy; raffaele.depalo@uniba.it
[3] National Research Council of Italy, IFN CNR, Institute for Photonics and Nanotechnologies, Via Amendola 173, 70125 Bari, Italy
* Correspondence: annalisa.volpe@poliba.it

Abstract: Carbon fibre-reinforced polymers (CFRP), thanks to their properties such as lightness, resistance to corrosion and fatigue, are emerging composite materials in the aeronautic fields, guaranteeing to reduce weight and costs by maintaining high performances in terms of strength and security. For preventing fluid damage and freezing, in aeronautic applications, CFRP parts need to be coated by painting. However, the paint/coating adhesion on CFRP composites is generally poor and affected by surface conditions. In this work, femtosecond laser texturing was investigated as an approach to improve adhesion of superhydrophobic coatings (SHC) to CFRP substrates. The laser textured surfaces show, after coating, a more lasting superhydrophobic behaviour compared to the as received sample, even after several cleaning cycles, demonstrating that the laser pre-treatment is a reliable and green method to enhance the adhesion of the SHC to the composite substrate.

Keywords: carbon fibre-reinforced composites; fs-laser; texturing; superhydrophobic coatings; adhesion; aerospace

Citation: Piscitelli, F.; De Palo, R.; Volpe, A. Enhancing Coating Adhesion on Fibre-Reinforced Composite by Femtosecond Laser Texturing. *Coatings* **2023**, *13*, 928. https://doi.org/10.3390/coatings13050928

Academic Editor: Chi Wai Chan

Received: 14 April 2023
Revised: 5 May 2023
Accepted: 11 May 2023
Published: 15 May 2023

1. Introduction

Carbon fibre-reinforced polymers (CFRP) offer significant advantages over metals in that they are lightweight, have high strength and stiffness, and are resistant to corrosion and fatigue [1]. These foretold properties make CFRPs favourable for a wide range of applications such as aerospace, automotive, electronics, rail transport, infrastructure, and renewable energy applications [2]. For aerospace, the two most recent long-range aircraft, the Airbus A350 and the Boeing 787, made extensive use of CFRPs in the airframe, over 50 wt%, in components such as wings, control elements, and fuselage parts [2]. The main advantage of using CFRP-based materials is connected to the possibility of deeply reducing weight and costs by maintaining high performances in terms of strength and security. The second major advantage depends on the possibility that they could be proper designed to guarantee the services they are made to [3].

To make the most of the peculiarities of these materials, carbon fibre composite parts need to be coated by paint [4]. In addition to aesthetics, image, and camouflage reasons, one of the most important reasons for painting, in particular in aeronautic applications, is the prevention of fluid damage [5]. Some resins are affected by prolonged water contact and freeze/thaw action can be damaging to the composite structure. The right paint system will provide a moisture barrier and protect the composite from damaging fluids such as hydraulic fluid and fuel [6]. Moreover, for CFRP composite, painting is often required to protect the surface from long-term UV irradiation that may decompose the polymeric matrix [7], resulting in exposure of carbon fibres which contributes to the failure of the composite. In addition to traditional paints [8,9], other functional coatings are emerging in aeronautic [10,11]. Recently, the use of passive ice protection systems (IPS) [12]

in combination with active ones, such as electro-mechanic [13], electro-thermal [14], or pneumatic [15], represents a promising solution to reduce the power supply of active IPS or limit the negative effect of icing conditions for drone applications [16]. Despite the main role in aeronautic application as passive ice protection is certainly that of the coating, a better adhesion of the coating to the surface is mandatory for preserving its properties as long as possible also in extreme conditions such as those encountered in flight with exposure to the elements. Unfortunately, the paint/coating adhesion on CFRP composites is generally poor and affected by surface conditions [17]. For example, the parts can be contaminated by mould release agents which frequently contain silicones. In order to ensure reliable painting, these contaminants must be removed completely. Only then, it is guaranteed that subsequent painting or bonding tasks will meet the highest standards of quality [18]. In addition to that, the mechanisms of paint/coatings adhesion are essentially connected to the concepts of surface roughness and surface wettability. Paint and coatings adhere to rougher surfaces more strongly because of the increased contact area and of an interlocking effect which holds paint/coating trapped. On the other hand, the improvement of adhesion between a paint/coating and a substrate at the interface is critically dependent on the improvement in wettability, and so, the surface wettability must be high to guarantee a good paint adhesion. This is because solids with high wettability, i.e., low water contact angles, have high surface free energy (e.g., metals) and tend to promote the adhesion of paints and better adsorb chemical coatings [19–21].

There are many surface treatment methods available for improving adhesion performance of composites. Such methods include sand-papering, corona discharge [22], plasma treatment [18], peel ply [23], grit blasting [24], and chemical cleaning. These techniques present several limitations. For example, sand-papering is a manual process that has poor control on the removal depth risking delamination defects and damaging the fibres and the bulk composite. Chemical methods with solvents, strong acids or bases, or ammonia treatment result in safety and environmental risks. Corona discharge and plasma treatments remove surface contaminants, roughen the surface, and introduce oxygen functional groups onto the composite surface, resulting in improved wettability of the surface. However, plasma treatment requires vacuum chambers that limit the size of the components to be treated. Thus, as each of these treatments have limitations, an alternative treatment should be provided.

Laser surface treatment became an important alternative to most traditional techniques and was accepted by many industries, due to ease of automation, reliability, high precision, process flexibility, non-contact, and environmental friendliness [25]. In particular, laser texturing was demonstrated to be an excellent method to modify surface wettability of many different materials, from polymers [26,27] to metals [28,29], by changing the surface topography and/or chemistry [30]. Laser technique is able to create a wide variety of surface topographies, both at the micro and nanoscales [31,32], with large repeatability, with excellent control of the surface features shape and size, and with a minimum affectation of the bulk material, then, making this technique attractive to treat materials sensitive to mechanical damage [33].

Although the effects of laser surface treatment in paint adhesion on CFRP surface was investigated by the point of view of changing in contact angle and chemical composition [17]; so far, no work was reported on the improvement of the lasting of coatings on laser-treated surfaces as cleaning cycles increase. In this contest, the aim of the present work is to study the effect of femtosecond laser (fs-laser) surface micromachining on the evolution of the adhesion of a superhydrophobic coating (SHC) applied on CFRP. Firstly, the influence of the fs-laser texturing on the wettability of the CFRP substrate was investigated. Then, the coating was applied to all samples. The adhesion of SHC was evaluated in static and dynamic mode as the cleaning steps increased and compared with the untreated surface. The coated laser-treated surfaces exhibited a more durable and reliable superhydrophobic behaviour than the non-textured one after several cleaning steps, representing a

promising green alternative to traditional methods for the enhancement of paint adhesion on CFRP materials.

2. Materials and Methods

2.1. Laser Texturing Apparatus

The laser processing apparatus used in this work is represented in Figure 1. The laser source employed was a Pharos SP 1.5 from Light Conversion. This source (M2 = 1.3, certified by the producing company) emitted 200 fs pulses centred around a wavelength of λ = 1030 nm. The maximum average power was of 6 W, resulting in a maximum pulse energy of E_P = 1.5 mJ and the pulse repetition rate was tuneable from single pulse to 1 MHz. The power of the linearly polarized laser beam was finely tuned by a half-wave plate coupled with a polarizer. The beam was then sent to a PC-controlled galvo scanner (SCANLAB intelliSCANSE 14, SCAN-LAB, Puchheim, Germany) on which a 100 mm F-theta lens was mounted. The upper surface of the sample was placed on the focal plane of this lens and the estimated beam waist w in air was 30 µm.

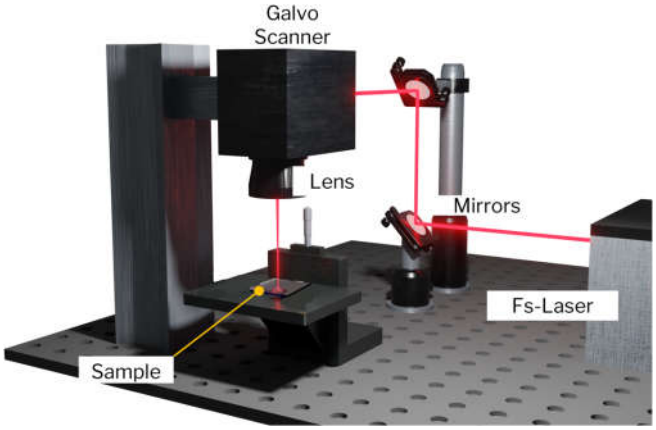

Figure 1. Setup for sample micromachining. The femtosecond laser beam was moved over the sample through a galvo scanner provided of a f-theta lens.

Immediately after laser processing and without other treatments, the samples were characterized using a scanning electron microscope (SEM) from Zeiss (Mod Sigma, Germany), which was used to both acquire images of the processed area and to perform an energy-dispersive x-ray analysis (EDX). The latter was used to obtain information about the chemical composition of the un-textured and textured surfaces.

Finally, the surface roughness of both the pristine and processed material was measured using an optical microscope (ContourGT-I 3D, Bruker, MA, USA) in profilometry mode.

2.2. Coating

A nanostructured superhydrophobic coating (SHC) was applied with an aerograph using de-humified air at 3 bars, with a layer-by-layer technique on flat CFRP, and cured at 80 °C. The distance between the aerograph and samples were optimized in order to guarantee uniformity in the coating's thickness and weight. The exploited SHC was developed at CIRA starting from the formulation described in a previous work [34] and modified in order to improve its durability. In this regard, other details about the performed changes cannot be disseminated in this manuscript, as covered by patents [35,36].

The SHC was applied on the pristine sample (hereafter labelled as P), providing the coated sample C, and on the laser micromachined samples by means of 1 (L1), 2 (L2) and 3 (L3) loops, giving the L1-C, L2-C, and L3-C coated samples, respectively.

The optical images were acquired with a microscope USB Dino-Lite AM4815ZTL (Dino-Lite Europe, Almere, The Netherlands) at 40×.

The contact angle (CA) measurements were performed at 23 °C in compliance with the ASTM D7490–13 [37] standard, with 3 µL of water (H_2O), diiodomethane (D), and formamide (F) [38]. Contact angles were rapidly acquired, within 30 s of depositing the drop, to avoid changes in angles. At least 6 measurements were acquired and average values and standard deviations were reported. Therefore, the surface free energy (SFE) was calculated as sum of the polar and dispersive components. The detailed procedure of the calculation of SFE values was described by Piscitelli et al. in [38].

Cleaning of coated surfaces was performed with a tissue embedded of ethyl alcohol. At each step, a new tissue was employed. Wettability was measured after 5, 10, and 20 cleaning steps.

An estimation of the dynamic wettability was performed on C and L3-C samples installed on a 30° tilted support by falling down a distillated water droplet having a volume of 20 µL at 23 °C.

3. Results and Discussion

Figure 2a,c shows the pictures of pristine (P) and coated samples (C), respectively, along with the images of 3 µL water droplets and the measured values of water contact angles (WCA). It highlights that after the application of the SHC the WCA increased from 52 to 165°, the wettability of surface was consequently reduced. The optical images at 40× of magnification show that the weave of CFRP substrates remained visible also after the application of the coating (Figure 2b,d).

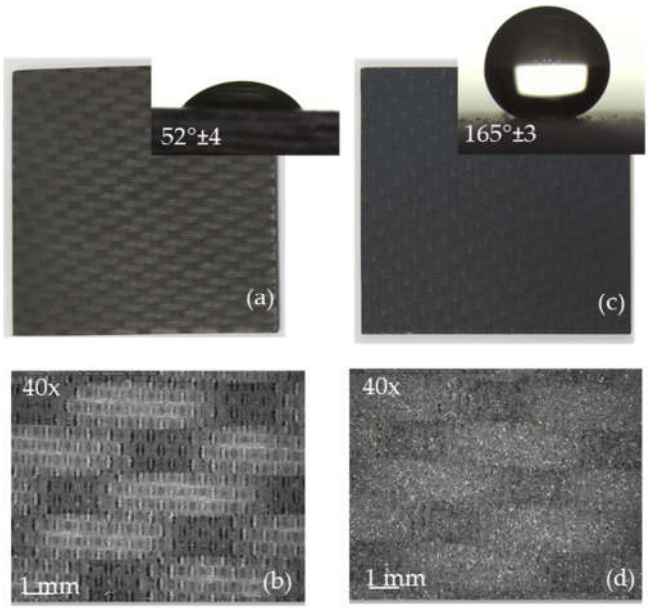

Figure 2. Pictures of pristine (**a**) and coated (**c**) samples; in the inserts the corresponding values of the WCAs were shown. The optical images at 40× of magnification of untreated (**b**) and coated (**d**) samples.

In Table 1, the laser parameters exploited for the texturing of the pristine substrate are reported. Three different samples were texturized, keeping fix all the parameters except for the number of consecutive loops. The beam was moved through the scanner following the cross-hatched path in Figure 3.

Table 1. Laser and process parameters involved in the production of the textured samples.

Wavelength	Pulse Duration	Pulse Energy	Scan Speed	Repetition Rate	Hatch *d*	Loops *L*
1030 nm	190 fs	12.5 µJ	0.5 m/s	200 kHz	10 µm	1-2-3

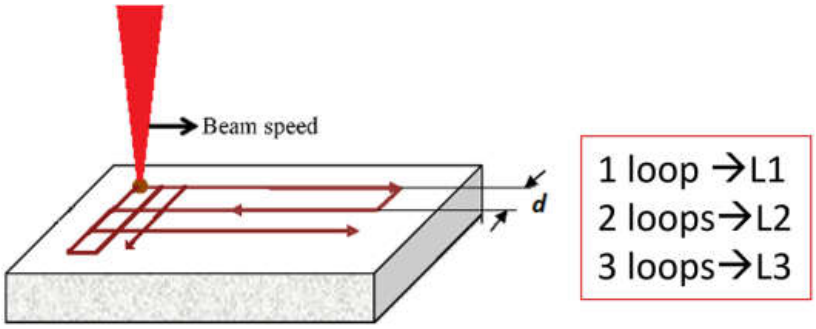

Figure 3. Crosshatch strategy. In the insert, the abbreviations for the machined samples are indicated.

In Figure 4, the SEM images of the samples after laser micromachining are compared with the pristine one. As can be seen from Figure 1b, a single loop was not enough to obtain a homogeneous surface, as residues of the epoxy resin layer remain. On the contrary, two and three loops allowed to completely uncover the texture of the fibres (Figure 4c,d). In Figure 4e,f, the surfaces machined after three laser passages were reported at two different magnifications. Although some more superficial fibres were broken, their surface structure was not affected by the passage of the laser.

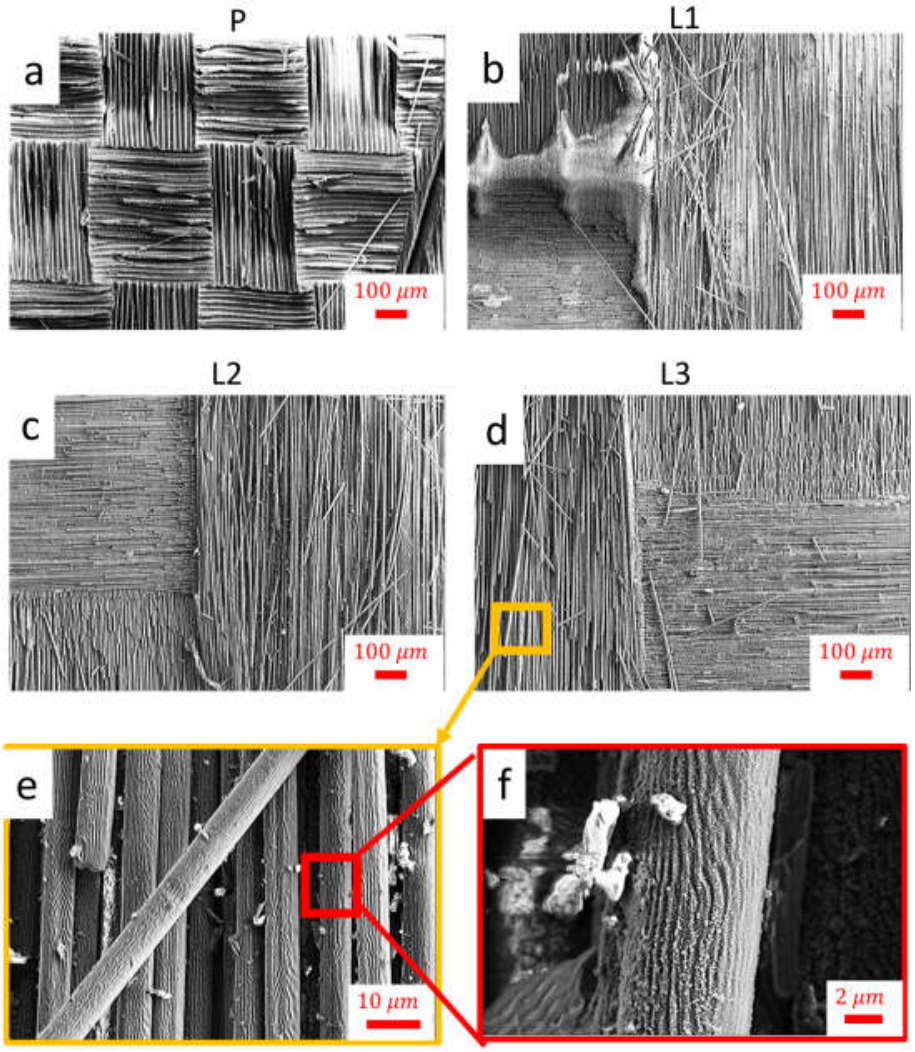

Figure 4. SEM images of the (**a**) untextured and (**b**–**d**) textured surfaces after with 1, 2, and 3 loops, respectively. (**e**) Magnification of the fibre structures after 3 loops with highlighted (**f**) a carbon fibre.

In Table 2, the corresponding roughness R_a and content of C and O obtained by optical profilometer and EDX analysis, respectively, are stated for each sample.

Table 2. Roughness values and C/O ratio of pristine and machined samples.

	P	L1	L2	L3
Ra (μm)	1.5 ± 0.2	4.8 ± 0.3	5.0 ± 0.2	5.3 ± 0.3
C/O (%)	2.9 ± 0.3	11.7 ± 0.2	23.7 ± 0.2	23.7 ± 0.2

The treated samples had an average roughness, R_a, more than three times higher than the untreated sample P. This can be ascribed to the ablation of the epoxy resin, leaving the structure of the carbon fibers uncovered. Moreover, the C/O ratio in all laser-treated samples was higher than the P surface, and the higher the laser loops number, the higher the C/O ratio, confirming that during the laser machining, the carbon fibres emerged. Meanwhile, epoxy resin was abraded, except for one loop where some epoxy resin remained [39].

In Table 3, the contact angles and the surface free energies of uncoated surfaces are reported. Compared to the pristine sample P, for which a WCA of 52° was measured, the laser micromachined samples L1, L2, and L3 showed lower WCA, which gradually reduced as the number of laser micromachining increased. In fact, average WCA values of 45°, 31°, and 25° were measured for L1, L2 and L3, respectively.

Table 3. Contact angles measured with water (H_2O), diiodomethane (D) and formamide (F) on pristine P and L1, L2, L3 laser-treated samples.

	P			L1			L2			L3		
	H_2O	**D**	**F**	**H_2O**	**D**	**F**	**H_2O**	**D**	**F**	**H_2O**	**D**	**F**
CONTACT ANGLE [°]	52 ± 4	28 ± 3	35 ± 3	45 ± 10	17 ± 3	29 ± 8	31 ± 4	13 ± 3	22 ± 5	25 ± 6	13 ± 3	22 ± 1
SFE [mN/m]		57.0			68.1			73.3			74.0	

As a consequence of the increased wettability, the SFE gradually increased from 68 to 74 mN/m as the number of laser micromachining increased. So, generally speaking, after the laser texturing, a hydrophilicity enhancement was reported. This effect was more evident for surfaces treated with two and three loops because, in the case of one loop, the epoxy resin was not homogeneously removed (see Figure 2b). An enhancement of the surface hydrophilicity after texturing, namely increasing the roughness, was in agreement with to the Wenzel equation [40]. For inherently smooth hydrophilic materials, i.e., at contact angles below 90°, it was demonstrated that, according to the principle that both hydrophobicity and hydrophilicity are reinforced by roughness [41], the increase in surface roughness was conducive to the wettability of water on the surface [42]. In fact, a rough material has a larger total surface area than a smooth one, due to the tiny depressions, and thus, in the Wenzel regime, offers a larger wetting area, with an increasing in wettability [43].

Afterwards, the coating was applied on L1, L2, and L3 laser micromachined samples, which from now on will be referred to as L1-C, L2-C, and L3-C samples, respectively.

Pictures of CFRP substrates L1, L2, and L3 prepared through laser ablation with 1, 2, or 3 loops are shown in Figure 5a–c and compared with same substrates after coating (Figure 5d–f). The laser micromachined area is the darker inner squares.

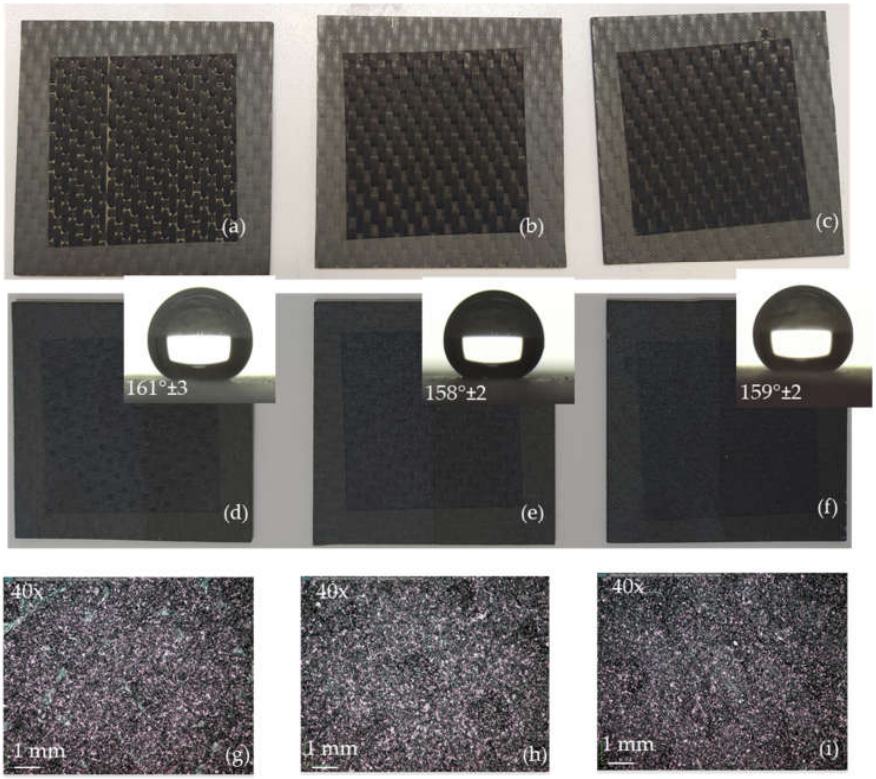

Figure 5. Samples after the laser micromachining: L1 (**a**), L2 (**b**) and L3 (**c**). Samples after the application of the SHC L1-C (**d**), L2-C (**e**), L3-C (**f**); in the inserts, images of water droplets and values of the contact angles are displayed; (**g**–**i**): corresponding optical images at 40× of magnification.

As shown in the insert of Figure 5d–f, after coating, all the surfaces became superhydrophobic with a measured WCAs between 158° and 161°.

In order to study the effect of the laser micromachining on the coating adhesion, all the samples were cleaned with tissue and ethyl alcohol up to 20 times.

In Table 4, the contact angles measured with water (H_2O), diiodomethane (D) and formamide (F) were reported at 23 °C before and after 5, 10, and 20 cycles of cleaning. Before cleaning, no significant difference in CA between untextured and textured coated samples was found. This effect can be ascribed to the uniformity of the applied coating, as displayed by the optical images in Figure 5g–i. So, it can be assessed that before cleaning, the roughness of the material on which the paint was applied did not influence the CA measurement. Conversely, a reduction in the CA with the cleaning can be observed for all samples. Figure 6 reports the percentage variation of water contact angles with respect to the uncleaned surfaces as a function of the cleaning cycles. The reduction was more pronounced for the C sample, i.e., −16, −20, and −24% at 5, 10, and 20 cleaning cycles, and less pronounced for the L3-C sample, for which reductions in the WCA of −6, −7, and −9%, respectively, were measured, proving a superior resistance of the SHC to cleaning on the laser-treated sample.

Table 4. Contact angles measured with water (H_2O), diiodomethane (D) and formamide (F) on pristine coated sample (C), and coated samples after laser micromachining (L1-C, L2-C, and L3-C).

	# CLEANING STEP											
	0			**5**			**10**			**20**		
CONTACT ANGLE [DEG]	**H_2O**	**D**	**F**	**H_2O**	**D**	**F**	**H_2O**	**D**	**F**	**H_2O**	**D**	**F**
C	165 ± 3	137 ± 8	141 ± 8	139 ± 7	89 ± 8	126 ± 6	132 ± 2	88 ± 3	128 ± 2	126 ± 5	86 ± 7	125 ± 8
L1-C	161 ± 3	136 ± 6	150 ± 5	144 ± 7	105 ± 9	134 ± 7	140 ± 1	111 ± 6	127 ± 3	133 ± 1	110 ± 12	120 ± 2
L2-C	156 ± 5	130 ± 8	147 ± 7	137 ± 3	111 ± 7	140 ± 6	142 ± 4	104 ± 2	126 ± 5	134 ± 3	101 ± 12	123 ± 4
L3-C	155 ± 8	125 ± 7	144 ± 8	146 ± 4	97 ± 12	138 ± 3	144 ± 6	111 ± 14	128 ± 5	140 ± 3	96 ± 7	133 ± 6

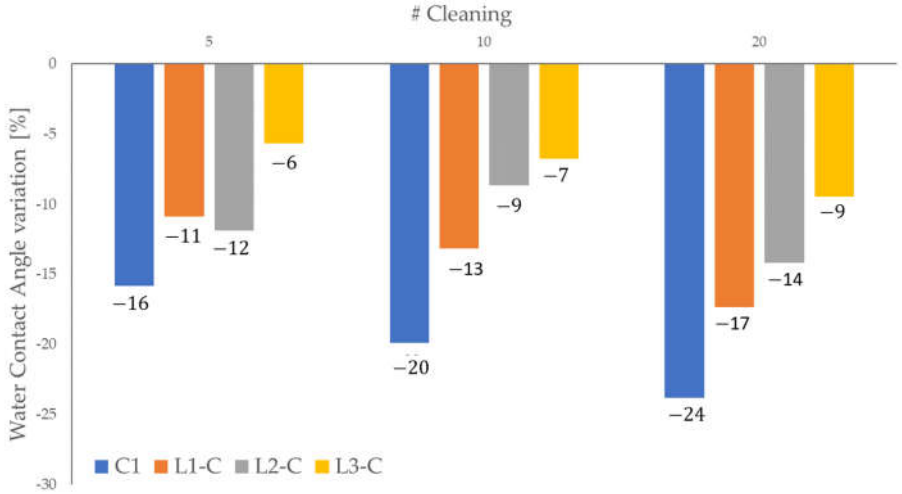

Figure 6. Percentage variations of the measured WCAs with respect the as-prepared samples.

Table 5 reports the calculated values of SFE for untreated and laser-treated coated samples, plotted in Figure 7 as percentage variations with respect to the uncleaned samples. According to the wettability trend, it highlights that for all samples, the SFE increased as the number of cleaning steps increased, especially for the L1-C and L2-C samples. The variations of SFE remained poor for C and, most of all, for L3-C sample. Additionally, it must be noted that the values of SFE assessed for all laser-treated samples, i.e., L1-C, L2-C, and L3-C, remained lower than that observed for the untreated coated sample C.

Table 5. SFE measured as-prepared and after 5, 10, and 20 cleaning steps on C, L1-C, L2-C, and L3-C samples.

# CLEANING STEP	0	5	10	20
	SFE [m/N/m]			
C	2.0	6.5	6.5	11.4
L1-C	0.5	4.0	5.5	7.5
L2-C	0.8	3.2	5.0	5.8
L3-C	1.5	3.0	4.2	5.5

Figure 7. Percentage variations of SFE with respect the as-prepared samples.

Figure 8 shows the optical images of samples after 20 cycles of cleaning along with the measurements of wettability in terms of WCA, highlighted in the inserts. From here, it emerged even more clearly how after cleaning the samples treated with the laser (L1-C, L2-C, and L3-C) retained their hydrophobic behaviour better than C. It is worth noting that after 20 cleaning cycles, the weave of composites became visible also for the laser-treated coated samples.

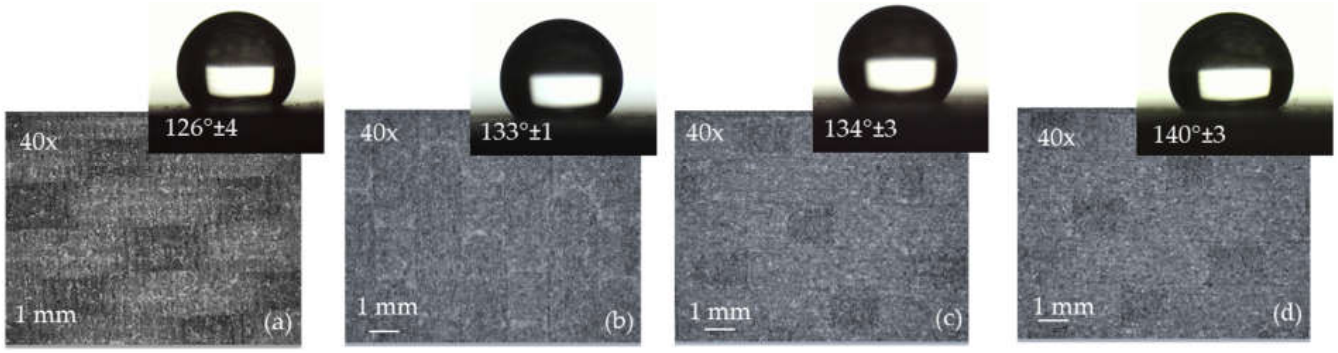

Figure 8. Microscope images at 40× of magnifications of C (**a**), L1-C (**b**), L2-C (**c**), and L3-C (**d**) samples after 20 cleaning steps. In the insert, images of water droplets along with the corresponding values of WCAs are reported.

To have an assessment of the dynamic wettability of the surfaces after the cleaning cycles, and then an estimation of the surface to repel impacting water droplets, the samples were positioned on a support tilted at 30°and allowing a water droplet with a volume of 20 µL to drop down on the surfaces. Figure 8 shows the image frames acquired before the cleaning cycles during the test performed on C sample (Figure 9a–c) and on L3-C sample (Figure 9d–f). In both cases, the characteristic behaviour of the water droplets impacting a superhydrophobic surface can be observed [44,45]. In fact, the water impacting the tilted surface assumed a pancake shape and rebound after the impact. The same behaviour was observed for the L1-C and L2-C samples; data are not shown here for brevity. Figure 10 shows the sequence of images acquired after 20 cycles of cleaning performed on the C (Figure 10a–c) and on L3-C (Figure 10e–g) samples. This highlights that after the 20 cleaning cycles, the water droplet impacting the tilted C sample adhered to the surface after impact; differently, the water droplet slid/rolled when it impacted the tilted L3-C sample. This means that the L3-C preserved the surface superhydrophobicity, unlike the C sample. Hence, for C sample, after 20 cleaning cycles, the wetting state changed from Cassie–Baxter to Wenzel state, due to local liquid penetration into the surface cavities, a phenomenon typically referred to as impalement [46]. On the contrary, for laser-treated samples, the Cassie–Baxter state was preserved, meaning that the pre-treatment of the composite surface with laser improved the adhesion of the coating to the substrate, so preserving the coating's functionality after surface cleaning. This effect can be ascribed to the increased surface roughness of the CFRP substrate after laser treatment. Indeed, surface roughness/texturing can provide increased surface area, promoting bonding strength through mechanical interlocking of paint to composite. Moreover, a role in paint adhesion can be also attributed to an increasing in surface active functional groups. As previously stated in [17], from the XPS surface analysis, it emerged that, during the laser treatment, CFRP surface chemically reacted with other elements such as oxygen and nitrogen from air forming active functional groups. The existence of active functional groups on the laser-textured CFRP surfaces improved paint adhesion [47], contributing, with the increase in roughness, to enhance the resistance of the coating to cleaning.

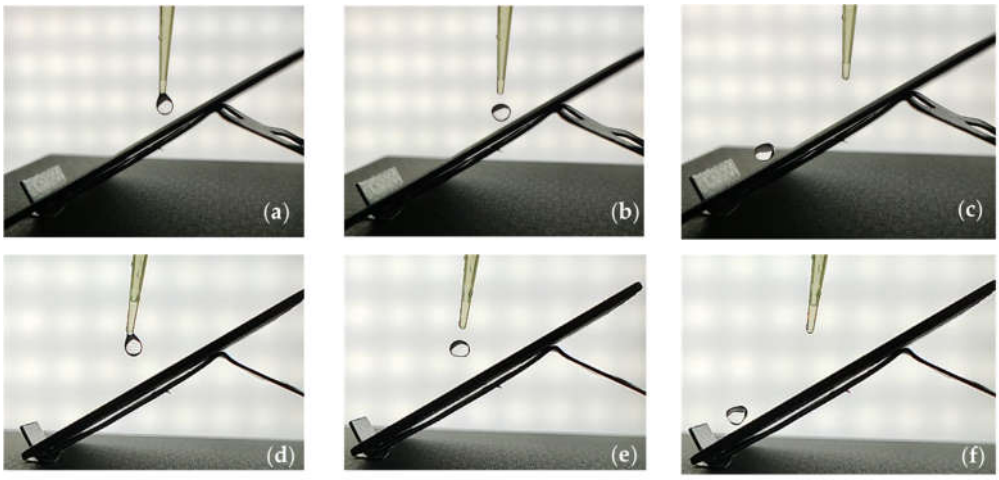

Figure 9. Images frames of 20 μL water droplets impacting the 30° tilted C (**a**–**c**) and L3-C (**d**–**f**) samples before the cleaning cycles (as-prepared samples).

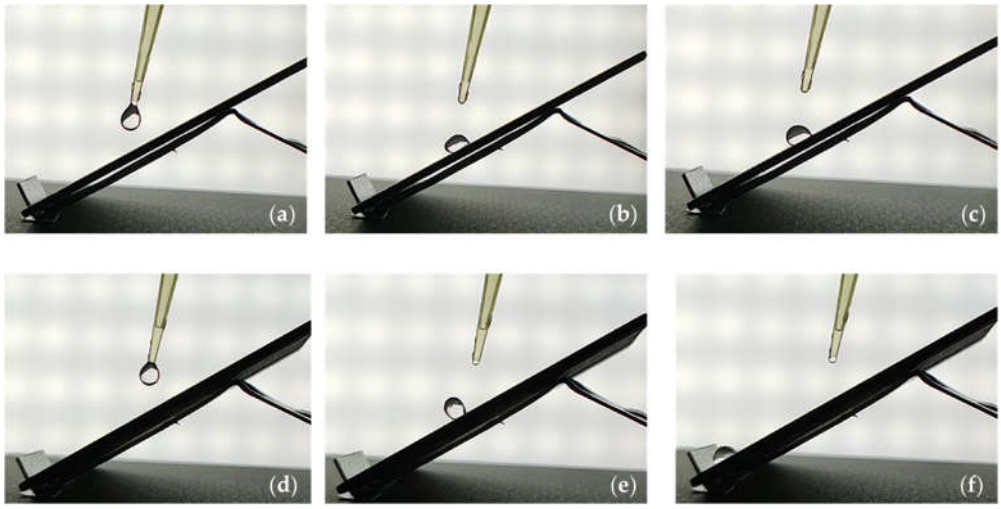

Figure 10. Images frames of 20 μL water droplets impacting the 30° tilted C (**a**–**c**) and L3-C (**d**–**f**) samples after 20 cleaning cycles.

4. Conclusions

In this work, the enhancement of the adhesion of a superhydrophobic coating (SHC) on CFRP through fs-laser micromachining was investigated. Three CFRP samples (L1-L2-L3) were textured using the same crosshatch strategy, differentiating only in the number of consecutive applications of the laser pattern, from 1 to 3. All the textured samples showed an increased surface roughness, with a reduction in CA and an increasing in SFE than the pristine material. An SHC was then applied on the textured samples. The coating adhesion was investigated by measuring the variations in WCA and SFE of the samples after increasing numbers of cleaning cycles (from 5 to 20), founding a lower percentage variation of both values, for the sample treated with 3 laser passages. Moreover, we found that, after 20 cleaning cycles, the water droplets slid/rolled when impacting the tilted textured sample, but adhered to the untextured one, proving the longest duration of the coating on the laser-treated sample.

These results demonstrate the fs-laser texturing is an effective tool for enhancing the adhesion between CFRP and SHC, so preserving the coating's functionality also after cleaning, offering a reliable and environmentally friendly solution, as it does not require additional chemical, to surface pre-treatment.

5. Patents

Data reported in this manuscript refer to coatings for which the formulation is protected by the patent submission: F. Piscitelli, Italian Patent Application N. IT102021000032444, "Rivestimento superidrofobico e ghiacciofobico di un substrato, metodo per il suo ottenimento e substrato così rivestito", 23 December 2021, and F. Piscitelli, F. Substrate superhydrophobic and icephobic coating, method for obtaining it and substrate thus coated, International Patent Application N° PCT/IB2022/062672 22 December 2022.

Author Contributions: Conceptualization, F.P. and A.V.; Experimental, F.P., R.D.P. and A.V.; methodology, F.P.; investigation, data curation, writing—review and editing, F.P., R.D.P. and A.V.; All authors have read and agreed to the published version of the manuscript.

Funding: This research received no external funding.

Institutional Review Board Statement: Not applicable.

Informed Consent Statement: Not applicable.

Data Availability Statement: Not applicable.

Acknowledgments: F.P. would like to thank Mario Costantini for his support in the acquisition of wettability measurements. A.V. would like to express her gratitude to Antonio Ancona, who generously provided knowledge and expertise.

Conflicts of Interest: The authors declare no conflict of interest.

References

1. Siddiquee, S.; Hong, M.G.J.; Rahman, M.M. *Composite Materials: Applications in Engineering, Biomedicine and Food Science*; Siddiquee, S., Hong, M.G.J., Rahman, M.M., Eds.; Springer: Cham, Switzerland, 2020.
2. Zhang, J.; Lin, G.; Vaidya, U.; Wang, H. Past, Present and Future Prospective of Global Carbon Fibre Composite Developments and Applications. *Compos. B Eng.* **2023**, *250*, 110463. [CrossRef]
3. Barile, C.; Casavola, C.; de Cillis, F. Mechanical Comparison of New Composite Materials for Aerospace Applications. *Compos. B Eng.* **2019**, *162*, 122–128. [CrossRef]
4. Mike Richardson Coatings for Composites. Available online: https://www.aero-mag.com/coatings-for-composites/ (accessed on 5 May 2023).
5. Sala, G. Composite Degradation Due to Fluid Absorption. *Compos. Part. B* **2000**, *31*, 357–373. [CrossRef]
6. Shunmugapriya, K.; Shirish, S.; Kale, G.; Gouda, P.; Jayapal, K. Tamilmani Paints for Aerospace Applications. In *Aerospace Materials and Material Technologies*; Prasad, N.E., Wanhill, R.J.H., Eds.; Springer: Singapore, 2016; Volume 1, pp. 539–562.
7. Smith, C.T.G.; Delkowki, M.; Anguita, J.V.; Cox, D.C.; Haas, C.; Silva, S.R.P. Complete Atomic Oxygen and UV Protection for Polymer and Composite Materials in a Low Earth Orbit. *ACS Appl. Mater. Interfaces* **2021**, *13*, 6670–6677. [CrossRef] [PubMed]
8. Prapan, C.; Sukantarat, C.; Maneephrom, T. Painting for Aircraft. *Proceedings* **2019**, *39*, 21. [CrossRef]
9. La Nasa, J.; Blaensdorf, C.; Dolcher, E.; Del Seppia, S.; Micheluz, A.; Modugno, F.; Pamplona, M.; Bonaduce, I. Historical Aircraft Paints: Analytical Pyrolysis for the Identification of Paint Binders Used on Two Messerschmitt Bf 109 Planes. *J. Anal. Appl. Pyrolysis* **2022**, *163*, 105468. [CrossRef]
10. Ghosh, S.K. *Functional Coatings and Microencapsulation: A General Perspective*; Wiley-VCH: Weinheim, Germany, 2006; p. 357. ISBN 352731296X.
11. Iroh, J.O.; Zhu, Y.; Shah, K.; Levine, K.; Rajagopalan, R.; Uyar, T.; Donley, M.; Mantz, R.; Johnson, J.; Voevodin, N.N.; et al. Electrochemical Synthesis: A Novel Technique for Processing Multi-Functional Coatings. *Prog. Org. Coat.* **2003**, *47*, 365–375. [CrossRef]
12. Huang, X.; Tepylo, N.; Pommier-Budinger, V.; Budinger, M.; Bonaccurso, E.; Villedieu, P.; Bennani, L. A Survey of Icephobic Coatings and Their Potential Use in a Hybrid Coating/Active Ice Protection System for Aerospace Applications. *Progress. Aerosp. Sci.* **2019**, *105*, 74–97. [CrossRef]
13. Schulz, M.; Sinapius, M. Evaluation of Different Ice Adhesion Tests for Mechanical Deicing Systems. In Proceedings of the SAE Technical Paper 2015-01-2135. 2015. Available online: https://saemobilus.sae.org/content/2015-01-2135/ (accessed on 5 May 2023).
14. Zhao, Z.; Chen, H.; Liu, X.; Liu, H.; Zhang, D. Development of High-Efficient Synthetic Electric Heating Coating for Anti-Icing/de-Icing. *Surf. Coat. Technol.* **2018**, *349*, 340–346. [CrossRef]
15. Filburn, T. Anti-Ice and Deice Systems for Wings, Nacelles, and Instruments. In *Commercial Aviation in the Jet. Era and the Systems that Make it Possible*; Springer: Cham, Switzerland, 2019.
16. Villeneuve, E.; Samad, A.; Volat, C.; Béland, M.; Lapalme, M. Experimental Investigation of Icing Effects on a Hovering Drone Rotor Performance. *Drones* **2022**, *6*, 345. [CrossRef]

17. See, T.L.; Liu, Z.; Cheetham, S.; Dilworth, S.; Li, L. Laser Abrading of Carbon Fibre Reinforced Composite for Improving Paint Adhesion. *Appl. Phys. A Mater. Sci. Process.* **2014**, *117*, 1045–1054. [CrossRef]
18. Buske, C. Aircraft Painting: Efficient and Environmentally Friendly Pretreatment of Fibre-Composite Materials by Means of Innovative Process Technology. *Besser Lack.* **2008**, *9*, 5.
19. Dillingham, G.; Oakley, B.; Voast, P.J.V.; Shelley, P.H.; Blakley, R.L.; Smith, C.B. Quantitative Detection of Peel Ply Derived Contaminants via Wettability Measurements. *J. Adhes. Sci. Technol.* **2012**, *26*, 1563–1571. [CrossRef]
20. Asgharifar, M.; Kong, F.; Abramovitch, J.; Carlson, B.; Kovacevic, R. Wettability Characterization and Adhesion Enhancement of Arc-Treated Surface of Aluminum Alloys. *Int. J. Adv. Manuf. Technol.* **2014**, *71*, 1463–1481. [CrossRef]
21. Packham, D.E. Surface Energy, Surface Topography and Adhesion. *Int. J. Adhes. Adhes.* **2003**, *23*, 437–448. [CrossRef]
22. Ragoubi, M.; George, B.; Molina, S.; Bienaimé, D.; Merlin, A.; Hiver, J.M.; Dahoun, A. Effect of Corona Discharge Treatment on Mechanical and Thermal Properties of Composites Based on Miscanthus Fibres and Polylactic Acid or Polypropylene Matrix. *Compos. Part. A Appl. Sci. Manuf.* **2012**, *43*, 675–685. [CrossRef]
23. Kanerva, M.; Saarela, O. The Peel Ply Surface Treatment for Adhesive Bonding of Composites: A Review. *Int. J. Adhes. Adhes.* **2013**, *43*, 60–69. [CrossRef]
24. Avcu, E.; Yıldıran Avcu, Y.; Baştan, F.E.; Rehman, M.A.U.; Üstel, F.; Boccaccini, A.R. Tailoring the Surface Characteristics of Electrophoretically Deposited Chitosan-Based Bioactive Glass Composite Coatings on Titanium Implants via Grit Blasting. *Prog. Org. Coat.* **2018**, *123*, 362–373. [CrossRef]
25. Wang, Q.; Wang, H.; Zhu, Z.; Xiang, N.; Wang, Z.; Sun, G. Switchable Wettability Control of Titanium via Facile Nanosecond Laser-Based Surface Texturing. *Surf. Interfaces* **2021**, *24*, 101122. [CrossRef]
26. Pan, Z.; Cheng, F.; Zhao, B. Bio-Inspired Polymeric Structures with Special Wettability and Their Applications: An Overview. *Polymer* **2017**, *9*, 725. [CrossRef]
27. Wilson, A.; Jones, I.; Salamat-Zadeh, F.; Watts, J.F. Laser Surface Modification of Poly(Etheretherketone) to Enhance Surface Free Energy, Wettability and Adhesion. *Int. J. Adhes. Adhes.* **2015**, *62*, 69–77. [CrossRef]
28. Moldovan, E.R.; Doria, C.C.; Ocaña, J.L.; Baltes, L.S.; Stanciu, E.M.; Croitoru, C.; Pascu, A.; Roata, I.C.; Tierean, M.H. Wettability and Surface Roughness Analysis of Laser Surface Texturing of AISI 430 Stainless Steel. *Materials* **2022**, *15*, 2955. [CrossRef] [PubMed]
29. Volpe, A.; Gaudiuso, C.; Di Venere, L.; Licciulli, F.; Giordano, F.; Ancona, A. Direct Femtosecond Laser Fabrication of Superhydrophobic Aluminum Alloy Surfaces with Anti-Icing Properties. *Coatings* **2020**, *10*, 587. [CrossRef]
30. Volpe, A.; Covella, S.; Gaudiuso, C.; Ancona, A. Improving the Laser Texture Strategy to Get Superhydrophobic Aluminum Alloy Surfaces. *Coatings* **2021**, *11*, 369. [CrossRef]
31. De Palo, R.; Volpe, A.; Gaudiuso, C.; Patimisco, P.; Spagnolo, V.; Ancona, A. Threshold Fluence and Incubation during Multi-Pulse Ultrafast Laser Ablation of Quartz. *Opt. Express* **2022**, *30*, 44908–44917. [CrossRef]
32. Costa, H.L.; Schille, J.; Rosenkranz, A. Tailored Surface Textures to Increase Friction—A Review. *Friction* **2022**, *10*, 1285–1304. [CrossRef]
33. Riveiro, A.; Pou, P.; del Val, J.; Comesaña, R.; Arias-González, F.; Lusquiños, F.; Boutinguiza, M.; Quintero, F.; Badaoui, A.; Pou, J. Laser Texturing to Control the Wettability of Materials. *Procedia CIRP* **2020**, *94*, 879–884. [CrossRef]
34. Piscitelli, F.; Tescione, F.; Mazzola, L.; Bruno, G.; Lavorgna, M. On a Simplified Method to Produce Hydrophobic Coatings for Aeronautical Applications. *Appl. Surf. Sci.* **2019**, *472*, 71–81. [CrossRef]
35. Piscitelli, F. Substrate Superhydrophobic and Icephobic Coating, Method for Obtaining It and Substrate Thus Coated. International Patent Application N° PCT/IB2022/062672 2022, 22 December 2022.
36. Piscitelli, F. Rivestimento Superidrofobico e Ghiacciofobico Di Un Substrato, Metodo per Il Suo Ottenimento e Substrato Così Rivestito. Italian Patent Application N. IT102021000032444, 23 December 2021.
37. *ASTM D7490-13*; Standard Test Method for Measurement of the Surface Tension of Solid Coatings, Substrates and Pigments Using Contact Angle Measurements. American Society for Testing and Materials: West Conshohocken, PA, USA, 2013.
38. Piscitelli, F.; Chiariello, A.; Dabkowski, D.; Corraro, G.; Marra, F.; Di Palma, L. Superhydrophobic Coatings as Anti-Icing Systems for Small Aircraft. *Aerospace* **2020**, *7*, 2. [CrossRef]
39. Raza, M.S.; Datta, S.; Bule, B.; Saha, P. Parametric Study of Laser Cutting of Carbon Fibre Reinforced Polymer (CFRP) and the Effect of Fibre Orientation on Cutting Quality. *Adv. Mater. Process. Technol.* **2019**, *5*, 202–212. [CrossRef]
40. Wenzel, R.N. Resistance of Solid Surfaces to Wetting by Water. *Ind. Eng. Chem.* **1936**, *28*, 988–994. [CrossRef]
41. Quã, D. Rough Ideas on Wetting. *Phys. A Stat. Mech. Its Appl.* **2002**, *313*, 32–46.
42. Wang, X.; Zhang, Q. Role of Surface Roughness in the Wettability, Surface Energy and Flotation Kinetics of Calcite. *Powder Technol.* **2020**, *371*, 55–63. [CrossRef]
43. Bormashenko, E.Y. 11. Superhydrophobicity and Superoleophobicity: The Wenzel and Cassie Wetting Regimes. In *Physics of Wetting*; De Gruyter: Berlin, Germany, 2017; pp. 177–200.
44. Antonini, C.; Villa, F.; Marengo, M. Oblique Impacts of Water Drops onto Hydrophobic and Superhydrophobic Surfaces: Outcomes, Timing, and Rebound Maps. *Exp. Fluids* **2014**, *55*, 1713. [CrossRef]
45. Backholm, M.; Molpeceres, D.; Vuckovac, M.; Nurmi, H.; Hokkanen, M.J.; Jokinen, V.; Timonen, J.V.I.; Ras, R.H.A. Water Droplet Friction and Rolling Dynamics on Superhydrophobic Surfaces. *Commun. Mater.* **2020**, *1*, 64. [CrossRef]

46. Lambley, H.; Schutzius, T.M.; Poulikakos, D. Superhydrophobic Surfaces for Extreme Environmental Conditions. *Proc. Natl. Acad. Sci. USA* **2020**, *117*, 27188–27194. [CrossRef]
47. Awaja, F.; Gilbert, M.; Kelly, G.; Fox, B.; Pigram, P.J. Adhesion of Polymers. *Progress. Polym. Sci.* **2009**, *34*, 948–968. [CrossRef]